\$ SUPER

Contents lists available at ScienceDirect

# **Chemical Physics Letters**

journal homepage: www.elsevier.com/locate/cplett





# Quantum states of a confined hydrogen atom calculated in a basis of explicitly correlated Gaussians

Arunima Coomar<sup>a</sup>, Keith Jones<sup>a</sup>, Ludwik Adamowicz<sup>a,b,\*</sup>

- a Department of Chemistry and Biochemistry, University of Arizona, Tucson, AZ 85721, USA
- <sup>b</sup> Centre for Advanced Study (CAS), N-0271 Oslo, Norway

#### ARTICLE INFO

Keywords:
Trapped hydrogen atom
Non Born-Oppenheimer method
Explicitly correlated Gaussians
Ground and excited states calculations

# ABSTRACT

A quantum-mechanical model for describing a hydrogen atom confined to a soft-wall cuboidal potential energy trap is implemented. Explicitly correlated Gaussian functions are used to expand the hydrogen wave functions that are symmetry-adapted with respect to the symmetry elements of the trapping potential. The calculations are performed without assuming the Born-Oppenheimer approximation. The electronic and nuclear densities of the calculated states are visualized using one-particle density plots. The approach enables to describe the behavior of a trapped hydrogen atom and, when extended to multiple hydrogen molecules, has potential for application in the theoretical modeling of the hydrogen storage phenomenon.

# 1. Introduction

The hydrogen atom subjected to various confinement potentials, by impenetrable or partially penetrable walls of different geometrical shapes such as spherical, paraboloidal, or prolate spheroidal walls, has been the subject of several studies over the past 80 years [1–5]. The goal of all these studies has been to observe how atomic properties evolve as a function of the confinment. The studies also led to the interest in confined multi-electronic systems such as helium [6-10], Li<sub>2</sub> [11], and LiH [12]. These model systems have since then been successfully applied to study spherically confined atoms and ions embedded in a plasma environment [13-15], appearance of critical points in the Shannon entropy sum [16], induced electrical and magnetic properties [17–20], second-order phase transitions [21], ionization and excitation probabilities for a bound system suddenly released from a penetrable confinement [22], confined quantum systems [23], anharmonic effects in solids [24], and nuclear shell models [25]. The studies have also proved useful to study different properties such as polarizability [26,27], hyperpolarizability [9], dipole moment [28], hyperfine splitting [29–32], NMR shielding constants [31], electron (de) localizations [33], and chemical reactivity [34]. More examples of systems with confined atoms and molecules can be found, for example, in Refs. [35-37].

The solutions for systems subjected to a confinement potential have been achieved by employing a wide variety of analytical and numerical

methods. Most of these studies use Coulomb potentials in conjunction with hard-wall potentials. These latter potentials are characterized by values that reach infinity at the confinement boundary. For a spherical confinement potential with  $r_0$  as the radius of the confinement, a hard-wall potential can be written as [26]:

$$V_{conf}\left(r\right) = \begin{cases} 0 & \text{if } 0 \leqslant r \leqslant r_0 \\ +\infty & \text{if } r \geqslant r_0 \end{cases}. \tag{1}$$

Looking at the above equation, it is clear that there is a discontinuity at  $r_0$ . Therefore, the eigenfunctions of the Hamiltonian that employ this potential must vanish at the boundary, when  $r_i = r_0$  (for some coordinate i), thus satisfying the Dirichlet boundary conditions,  $\Psi(r_1,...,r_n) = 0$ , at the boundary surface.

The kind of confinement potentials discussed above is not very well suited to study traditional quantum-chemistry phenomena, which uses basis functions such as Gaussians that extend to infinity. To address these issues, Pasteka et al. suggested a soft-wall confinement potential [38]. The spherical confinement used by them to study *n*-electron systems in the Ref. [38] was:

$$V_{conf}\left(r_i\right) = \sum_{i=1}^n \left(\frac{r_i}{r_0}\right)^N,\tag{2}$$

where  $r_0$  is the radius of the confining sphere and  $N \in \mathbb{N}$  is the stiffness parameter that can control the penetrability of the sphere. Since  $V_{conf}(r_i)$ 

<sup>\*</sup> Corresponding author at: Department of Chemistry and Biochemistry, University of Arizona, Tucson, AZ 85721, USA.

E-mail addresses: acoomar@email.arizona.edu (A. Coomar), keith139@msn.com (K. Jones), ludwik@u.arizona.edu (L. Adamowicz).

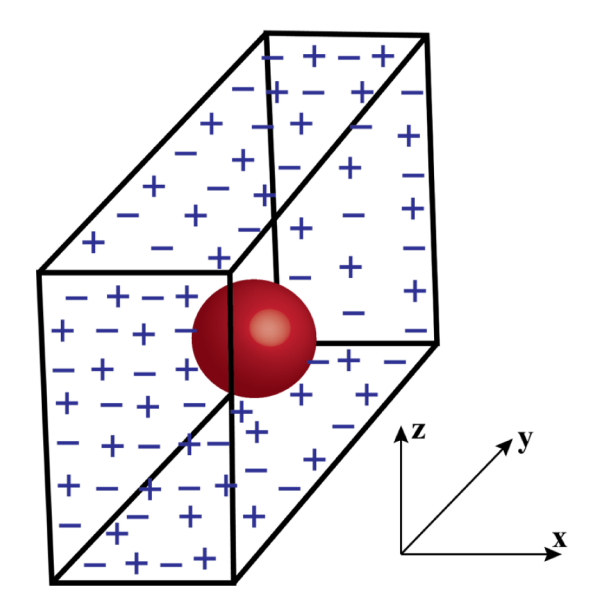


**Fig. 1.** A schematic representation of the system (not to scale). The red sphere represents the hydrogen atom trapped inside a cuboidal PE trap. The sides of this cuboid are of lengths 5 a.u., 20 a.u., and 10 a.u. along the x, y, and z-directions, respectively. There are 5402 point charges of unit magnitude distributed at equal density all along the surface of the cuboidal trap.

does not possess a discontinuity at  $r_0$ , there is no necessity to apply the Dirichlet boundary condition at  $r=r_0$ , simplifying its use with existing numerical algorithms and with standard Gaussian-based electronic-structure software packages. Even without the Dirichlet boundary condition applied to these systems, it can be expected that the wave functions will decay quite rapidly for  $|r_i| > r_0$ . The Pasteka potential was successfully employed by the authors of Ref. [38] to study the confinement of one electron hydrogen atom, as well as many-electron systems like helium, carbon, potassium, and methane.

In the present work, we develop a quantum mechanical model of a hydrogen atom trapped in a cuboidal "box" that is made up of alternating positive and negative point charges. This serves as a soft-wall confinement potential where we do not require the wave functions to vanish at the boundary. The quantum states of this single hydrogen atom interacting with the confinement potential are investigated using the effective non-Born-Oppenheimer (non-BO) method introduced by Kozlowski and Adamowicz [39]. The main tenet of this approach is treating the nuclei and electrons on an equal quantum-mechanical footing, whereby the BO approximation is not assumed. This means that the wave function for a particular state of the system depends on the coordinates of both types of particles comprising the said system. We employ explicitly correlated Gaussian (ECGs) functions with shifted centers to expand the spatial parts of the ground and excited-state wave functions of the trapped hydrogen. The approach facilitates an effective way to describe the coupled motion of the electron and the proton within the box without the BO approximation. As ECGs explicitly depend on all inter-particle distances, they enable to represent the correlated proton-electron motion to a high degree of accuracy. Though in the proof-of-concept scenario of a single hydrogen atom we do not have any nucleus-nucleus and electron-electron correlations, the ability to include them for more complex systems such as a hydrogen molecule or a cluster of hydrogen molecules is expected to give us more accurate results compared to techniques that employ orbital expansions of the wave functions of the electrons and the nuclei.

Another possible application of the work described in this work would be to model the hydrogen storage phenomenon for applications in the hydrogen economy. There are five key elements of the hydrogen economy infrastructure-production, delivery, storage, conversion, and application [40]. This concept was first introduced in the mid-1970s and

research into its viability has been steadily increasing, as the climatecrisis has quickly become one of the most important problems for the 21st century. The hydrogen economy improves the energy security and also reduces oil-spills, carbon dioxide and other greenhouse gas emissions, making it a perfect solution for the future [41]. While the five elements of the infrastructure are all in several stages of development [42], research on hydrogen storage is in the forefront, since developing safe, reliable, compact, and cost-effective materials for use in fuel-cell technology will lead to a greater viability of the hydrogen economy.

Important classes of materials considerd for hydrogen storage include: (i) carbonaceous materials like fullerenes, carbon nanotubes (CNTs) and graphene, (ii) metals and alloys (intermetallics), (iii) metal organic frameworks (MOFs) and covalent organic frameworks (COFs), (iv) zeolites, and (v) clathrates [43]. Multiple studies have been carried out to investigate the hydrogen storage characteristics of these materials to varying degrees of success. There have also been several experimental and theoretical studies on clathrate hydrates, preliminary explorations of which have shown that these materials could serve as the next revolutionary on-board hydrogen storage materials [44].

In this work, we consider not a cubic, but a cuboidal potential energy (PE) "box", as this provides a better model for trapping of a hydrogen atom in a cage formed by molecules of a clathrate. The cuboidal trap used in the present work is shown in Fig. 1. In a cuboidal box, where the x, y, and z dimensions are different, there are eight different types of angular symmetry states of a hydrogen atom or molecule placed within the "box". The reason for there being eight symmetry types of states arises from the following: with the center of the box located in the center of the coordinate system, the wave function can either be symmetric (S) or antisymmetric (A) with respect to the x plane, symmetric or antisymmetric with respect to the y plane, and symmetric or antisymmetric with respect to the z plane. Also, within each symmetry, there are states that differ in terms of the number of "radial" nodes in their wave functions. These "radial" states for each of the eight symmetries are calculated separately. For the purpose of visualizing all these different states, we use plots of the electronic and nuclear densities. These plots show us the relative distributions of the electron and the proton in the ground the excited states of the hydrogen atom confined to the potentialenergy trap. It is obvious that, in its nascent stage of development, our model cannot account for all the different facets of hydrogen storage. However, there are possible ways of extending the model so it can be ultimately used to study the hydrogen storage phenomenon.

### 2. The method

We need to expand the total spacial wave functions of the trapped hydrogen atom in terms of a set of *K* basis functions as:

$$\Psi\left(r\right) = \sum_{k=1}^{K} c_k \phi_k\left(r\right),\tag{3}$$

where  $\Psi$  is the wave function,  $\phi_k$ 's are the basis functions and the  $c_k$ 's are the linear expansion coefficients that determine how the different basis functions contribute to the overall wave function.

As mentioned, in the present calculations, we employ explicitly correlated gaussian (ECGs) functions with shifted centers, also known as floating explicitly correlated Gaussians (FECGs). Each of these ECGs can be written as the following *N*-particle Gaussian function:

$$\phi_{k}\left(r\right) = \prod_{i=1}^{N} \exp\left[-\alpha_{i}^{k} (r_{i} - R_{i}^{k})^{2}\right] \prod_{j>1}^{N} \exp\left[-\beta_{ij}^{k} (r_{i} - r_{j})^{2}\right]. \tag{4}$$

In the Eq. 4, the first term represents the N orbital Gaussians and the second term represents the N(N-1)/2 Gaussian pair functions or geminals.  $\alpha_i^k$  is the orbital exponential parameter of Gaussian k for particle i. Similarly,  $\beta_{ij}^k$  is the exponential parameter of the  $k^{th}$  Gaussian pair

function that is formed by particles i and j.  $r_i$  is the position vector of particle i, namely  $(x_i, y_i, z_i)$ , r is a vector of length 3N built from the  $r_i$  position vectors of the particles, and  $R_i^k$  is the center of the Gaussian k for particle i.

Eq. 4 can be alternatively written in the following simpler form which makes it easier to manipulate and optimize the non-linear parameters:

$$\phi_k(r) = \exp[-(r - s_k)'(A_k \otimes I_3)(r - s_k)]. \tag{5}$$

Here r is the same vector as explained previously. The prime symbol (′) is used to denote the vector and matrix transposition operation. In the case of the hydrogen atom, we have two particles, the proton and the electron, and N=2. For the hydrogen molecule, N=4, as we have 2 electrons and 2 protons in this case. In Eq. 5,  $s_k$  is a 3N-dimensional vector that contains the Gaussian shifts,  $A_k$  is an  $N\times N$  dimensional symmetric matrix of the Gaussian exponential parameters, and  $I_3$  is the  $3\times 3$  identity matrix. The Kronecker product of  $A_k$  with this identity matrix  $I_3$  gives us a  $3N\times 3N$  dimensional symmetric matrix.

Our previous work has shown that the ECG basis functions are spherically asymmetric, and can be made square integrable and form a complete set [45]. The reason why they are not spherically symmetric stems from the fact that the centers of these Gaussians are shifted away from the origin, making these shifts directional in nature. This property makes these basis sets ideal to be used when we want to study, for example, systems that are under the influence of external electric fields, or confined to a non-spehrical trap such as the one considered in this work. The method that is used to ensure the square integrability of the basis functions is discussed shortly.

In the non-BO approach, where the electrons and nuclei are treated equivalently in the calculations, the ECGs can effectively describe the electron-electron, electron-nucleus, and nucleus-nucleus correlation effects by including explicit dependence on the inter-particle distances,  $(r_i-r_j)$ , in Eq. 4. The latter two correlation effects are quite significant because the electrons, particularly the core electrons, have the tendency to follow the nuclei very closely and the nuclei tend to stay away from each other leading to a small overlap of their wave functions. Therefore, these two correlations are qualitatively different from those of the electrons, which, because of their lighter masses, typically create a significantly larger overlap of their wave functions.

In order to describe bound states of the system, auch as the types of states studied in the present work, Gaussians (Eq. 5) that are used to expand the corresponding wave functions need to be square integrable. This can only be achieved when  $A_k$  is positive definite. We get around this problem by constructing  $A_k$  from a lower-triangular  $N \times N$  matrix,  $L_k$ , using the following Cholesky factorization method:

$$A_k = L_k' L_k, \tag{6}$$

where

$$L_{k} = \begin{pmatrix} L_{k}(1,1) & 0 & 0 & \dots & 0 \\ L_{k}(1,2) & L_{k}(2,2) & 0 & \dots & 0 \\ L_{k}(1,3) & L_{k}(2,3) & L_{k}(3,3) & \dots & 0 \\ \dots & \dots & \dots & \dots \\ L_{k}(1,N) & L_{k}(2,N) & L_{k}(3,N) & \dots & L_{k}(N,N) \end{pmatrix}.$$

$$(7)$$

The elements of this  $L_k$  matrix can vary in the range  $[-\infty, +\infty]$  thus ensuring that, when we perform a variational optimization of the Gaussians, we can do so without putting any constraints on the  $L_k$  matrix elements. The variational adjustment of the  $L_k$  parameters (as well as the  $s_k$  coordinates), make the ECG functions flexible enough to represent the bound states of the trapped hydrogen systems under study in the present work.

We next present the non-BO Hamiltonian operator used in the calculations. In general, for q nuclei and n electrons (q+n=N). The Hamiltonian is:

$$\widehat{H} = \widehat{T} + \widehat{V} = -\nabla'_{r} M \nabla_{r} + \sum_{i=1}^{N} \sum_{j=i+1}^{N} \frac{q_{i} q_{j}}{r_{ij}} + \sum_{i=1}^{N} \sum_{j=1}^{M} \frac{q_{i} p_{j}}{s_{ij}},$$
(8)

where

$$\nabla_{r} = \begin{pmatrix} \frac{\delta}{\delta x_{1}} \\ \frac{\delta}{\delta y_{1}} \\ \frac{\delta}{\delta z_{1}} \\ \frac{\delta}{\delta z_{2}} \\ \vdots \\ \frac{\delta}{\delta z_{N}} \end{pmatrix}$$

$$(9)$$

and

$$M = \begin{pmatrix} \frac{1}{2m_{p1}} & 0 & 0 & 0 & \dots & 0 \\ 0 & \dots & 0 & 0 & \dots & 0 \\ 0 & 0 & \frac{1}{2m_{pq}} & 0 & \dots & 0 \\ 0 & 0 & 0 & \frac{1}{2m_{e1}} & \dots & 0 \\ \dots & \dots & \dots & \dots & \dots \\ 0 & 0 & 0 & 0 & \dots & \frac{1}{2m_{en}} \end{pmatrix}. \tag{10}$$

Here,  $\widehat{T}$  and  $\widehat{V}$  are the kinetic and potential energy operators respectively and  $\nabla_r$  is the gradient operator. The kinetic energy operator,  $\widehat{T}$ , includes an  $N \times N$  diagonal mass matrix M. This matrix contains the masses of the q nuclei,  $m_{p1}, m_{p2}, \cdots, m_{pq}$ , in the first q diagonal elements and the masses of the n electrons,  $m_{e1}, m_{e2}, \cdots, m_{en}$ , in the next n diagonal elements. The total numbers of the q nuclei and the n electrons add up to N. The potential energy operator,  $\widehat{V}$ , is made up of two terms. The first term represents the interaction between the N particles and the second term corresponds to the interaction between the N particles in the system and the M point charges located on the surface of the cuboidal PE trap.  $q_i$  is the charge of particle i,  $r_{ij}$  is the distance between the particles i and j,  $p_j$ ,  $j=1,\ldots,M$ , are the point charges uniformly distributed on the surface of the cuboid trap, and  $s_{ij}$  is the distance between particle i and point charge j. Thus, term  $\sum_{i=1}^N \sum_{j=1}^{M} \frac{q_i p_j}{s_{ij}}$  in (8) represents the trapping potential in the present calculations.

In the present calculations, we use the standard variational method to obtain the energies of the states and their corresponding wave functions. This is done by minimizing the energy with respect to the linear expansion coefficients of the wave function in terms of the basis functions,  $c_k$ 's, the  $L_k$  matrix elements and the coordinates of the shift vector  $s_k$ . For a system formed by N particles, each N-particle Gaussian basis function has a total of  $3N s_k$  parameters and  $N(N+1)/2 L_k$  parameters, as well as one  $c_k$  parameter. For the hydrogen atom, we thus have three  $L_k$  matrix elements, six  $s_k$  coordinates, and one  $c_k$  parameter for each ECG basis function in the wave function of each state. These parameters are optimized for each basis function by variational minimization of the total energy:

$$E\left[\Psi\right] = \min_{L_k, s_k, c_k} \frac{\langle \Psi | \widehat{H} | \Psi \rangle}{\langle \Psi | \Psi \rangle}. \tag{11}$$

In the energy minimization, the energy gradient determined with respect to all  $L_k$  and  $s_k$  parameters is employed [45]. The use of the

gradients significantly accelerates the minimization process.

As mentioned, the probability densities of the electron and the proton in the ground and excited states of the system are calculated and analyzed. In general, the one-particle density of particle one can be calculated by the method outlined in the previous work from our lab [45]. This standard procedure to calculate the particle-one density involves squaring the wave function,  $\Psi^*\Psi$ , and then integrating over the coordinates of all the particles  $(2,3,\cdots,N)$  other than particle one:

$$P(r_1, r_1') = \int \Psi(r_1, r_2, ..., r_N) \Psi(r_1', r_2, ..., r_N) dr_2, ..., dr_N.$$
 (12)

In order to calculate the density of any particle other than the first particle, i.e. particle i, we simply interchange the position of that particle with the first particle in the wave function. This is easily done by exchanging the appropriate rows and columns of the  $A_k$  matrix (and the corresponding coordinates of the  $s_k$  vector) so that particle i becomes particle one and particle one becomes particle i. After the densities are calculated in this manner, they are plotted using the 3D-xy contour plot feature embedded in Mathematica.

#### 3. Illustrative calculations

The hydrogen atom is placed in a cuboidal potential energy trap (the potential energy "box") that has the dimensions of 5 atomic units (a.u.) along the x-direction, 20 a.u. along the y-direction, and 10 a.u. along the z-direction, with the center of the cuboid located at the origin (0,0,0) of the coordinate system. A schematic picture of this box is presented in Fig. 1. Point charges of unit magnitude having alternate signs are placed all along the faces of this cuboidal box. There are a total of 5402 charges of alternating sign distributed at equal intervals along the whole surface area of the cuboidal potential energy trap. The lengths of the three sides, the charge magnitude, and the charge density are all tunable parameters in our calculations.

As mentioned, the reason for choosing a cuboidal box is to ensure that the model depicts a real system of a trapped hydrogen atom better than a cubic box would. In reality, a hydrogen atom is entrapped in a cavity formed by a molecular network. To a first degree of approximation, we simulate the presence of the molecules forming the cavity with the "point charges". For most situations, these molecules will not be creating an uniform "cubic box" but would rather more closely resemble a cuboidal trap. Therefore, using an PE trap that has unequal lengths along the three axes seems to be a better first-order approximation. This cuboidal box also causes the system to have a lesser degree of degeneracy of the energy states. Due to this, we are able to access a particular individual energy level for closer inspection more easily than would be possible if multiple states had the same energy.

The calculations starts with a basis set of three ECGs describing a hydrogen atom located in the first quadrant of the box, i.e. the quadrant with x>0, y>0, and z>0. These "generator" ECGs have all their centers shifted slightly away from the origin (0,0,0). We then use each of these generator functions to create 8 symmetry-reflected Gaussian functions according to the procedure described below.

In the current problem, there are three symmetry planes (x,y), and z) from which we can create eight different reflection combinations. A non-BO wave function describing a state of the hydrogen atom in the box that is symmetric along all the three planes is labeled as SSS. Wave functions can also have one plane along which the reflection is antisymmetric. If the wave function is antisymmetric with respect to the x-plane, we label it ASS. Similarly, if the wave function is antisymmetric with respect to the y- and z-planes, we label it SAS and SSA, respectively. A wave functions can also have two antisymmetry planes. If the antisymmetry planes are the x and y planes, we label it AAS. Analogically, a ASA wave function has antisymmetry along x and z planes and a SAA wave function only has one symmetric plane, namely the x-plane. The eighth and final combination is the case where the wave function is simultaneously

**Table 1**The minimized energies of the lowest states of the hydrogen atom for eight angular symmetries. The minimized energies of the lowest states of the eight angular symmetries calculated using the variational method.

Angular Symmetry State	Minimized Energy (in Hartree)
SSS	-0.496562
SAS	-0.496507
SSA	-0.496445
ASS	-0.496446
ASA	-0.496442
AAS	-0.496376
SAA	-0.496401
AAA	-0.496327

antisymmetric along all the three planes and we label it as AAA.

Each "generator" Gaussian function is reflected along the three symmetry planes to create the eight functions. Next, the eight functions are used to form linear combinations with appropriate linear expansion coefficients corresponding to the particular symmetry. In this way a symmetry-adapted basis set is constructed. Therefore, if we start with three generator ECGs, we, in effect, have  $3\times 8=24$  symmetry-adapted Gaussian functions in the basis set. Each of the generator Gaussian functions have 2(2+1)/2=3  $L_k$  parameters and  $3\times 2=6$   $s_k$  parameters. The three generator Gaussians also have three  $c_k$  coefficients. Therefore, we have a total of 10 adjustable linear  $(c_k)$  and non-linear  $(L_k)$  and  $s_k$  parameters per ECG function. In this way we create the basis set for the calculation.

Once we have a basis set, we use our in-house code to carry out a variational minimization of the energy of the lowest-energy state for each of the eight symmetries with respect to the parameters  $L_k, s_k$ , and  $c_k$ . The minimization employs an algorithm that utilizes the analytical energy gradient determined with respect to all these non-linear parameters. The energies of the lowest states of the eight different angular symmetries calculated in this way are presented in the Table 1.

If all these states are optimized to the same level of convergence, as is done in our calculations, we would expect the lowest energy state to be the one that is symmetric with respect to all three planes, i.e., the SSS state, while the highest energy state among the lowest energy states of the eight symmetries would be the AAA state. Also, most states with one symmetry plane (ASS, SAS and SSA) are expected to have lower energies than ones with two antisymmetry planes (AAS, ASA and SAA). This is exactly what we get from the calculations as evidenced from the Table 1.

At this point, it is worthwhile to note that working with atoms and molecules in confinement potentials can lead to linear dependencies between the basis functions, since all these basis functions are constrained within a small spatial area [46-49]. Linear dependencies arise when the overlap between two basis functions, i and j, i.e.,  $S_{ij}$ , is too close to one. As this may lead to numerical instabilities and inaccuracies in the calculations, it is imperative that we remove such linear dependencies. The way we deal with this in our calculations is by having a threshold value specified for the overlap,  $S_{ij} = 0.99$  and by using a cyclic optimization procedure [50]. In this cyclic optimization procedure, basis functions are optimized one function at a time, meaning that the  $L_k$  and  $s_k$  values of that function are the only parameters that are optimized in the calculations and all other  $L_k$  and  $s_k$  values are frozen. The optimization is carried out over several cycles. In this work, the number of cycles chosen is 20 for each basis function. At the end of each optimization cycle of the function, if the calculation finds that it has an overlap equal to or greater than 0.99 with any other function(s), it marks it as being linearly dependent and when that happens, the program resets the value of the parameters of this basis function back to its original preoptimization values. This back-tracking is not problematic because, by the time the next cycle arrives, the entire energy hypersurface will have changed due to the optimization of the other functions. In this new cycle, that basis function may no longer be linearly dependent on the other function(s) and its optimization may proceed without any issues. A

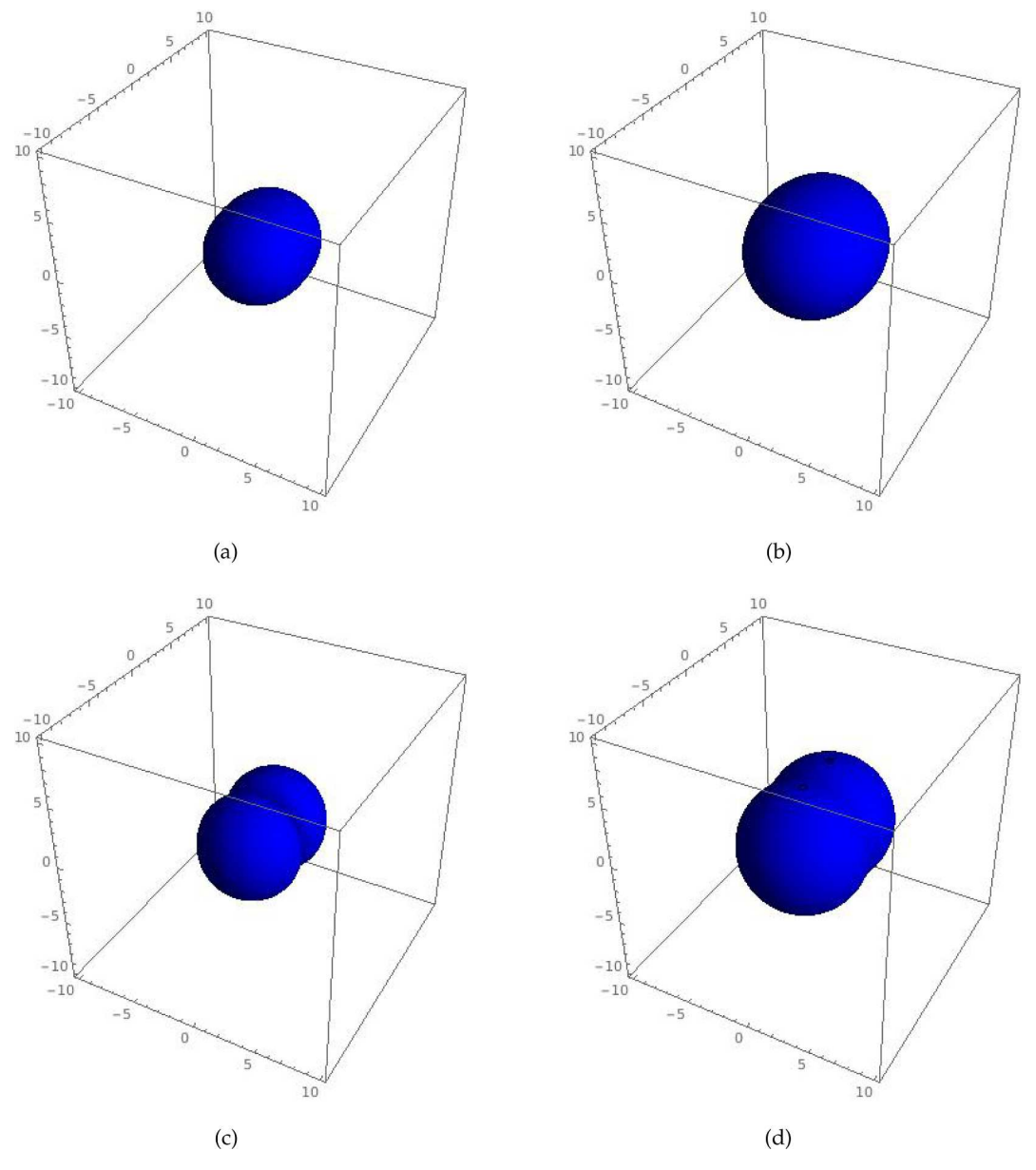


Fig. 2. Contour plots of (a) proton density and (b) electron density for the lowest SSS state; Contour plots of (c) proton density and (d) electron density for the lowest SAS state. The contour value used in plots (a)-(c) is 0.0003.

pairwise linear dependency can also manifest itself by two different basis functions having very similar and large values of the linear coefficient, but with opposite signs. This kind of pairwise linear dependencies can also be located and efficiently removed by making use of the Schmidt orthogonalization routine outlined in detail in [50]. Thus we can see that if we begin our calculations with basis functions that are sufficiently different from each other, the calculation can ensure that linear dependencies can be taken care of, while maintaining the integrity of the basis set.

In the Fig. 2–5, we present the 3-dimensional plots of the electron and proton densities of the eight angular symmetry states. The density calculations are performed in a cubic box whose length coincides with the longest side of the cuboid trapping potential. Due to the limitations of the plotting software used in this work, we plot the densities using a cubic box rather than a cuboidal box. The use of the cubic box with larger parameters than those of the cuboidal box representing the trap allows us to check whether there is any appreciable amount of the electronic or nuclear density that tunnels out of the box. Upon examining the plots, no tunneling of the densities out of the cuboidal trap is

found.

The cubic box used in the density calculations has dimensions  $20\times20\times20$  atomic units (a.u.) and a grid with a step size of 0.5 a.u along all the axes is used in the plotting. The center of the coordinate system coincides with the center of the box, so each of the edges in our calculation starts at -10 a.u and ends at +10.u. The total number of points in such a cubic box where the density is calculated is thus  $41^3=68921$ . Once the calculation of the density is completed, it is numerically integrated over the whole cubic box to check what part of the wave function is located within the box. For the ground-state calculations, a desirable result of this integration should be a number close to one. Our test shows that this is indeed what happens. We present the numerical-integration values for all the eight symmetry states in the tables below. Table 2 lists the values of the integrated densities of the proton while Table 3 lists those of the electron.

A test calculation of the densities using a grid size of 0.25 a.u. along the longest axis (i.e., the *y*-axis) was also done to check the convergence of the results with grid size. This calculation, understandably, took more computational time, but it did not change the integrated value of the

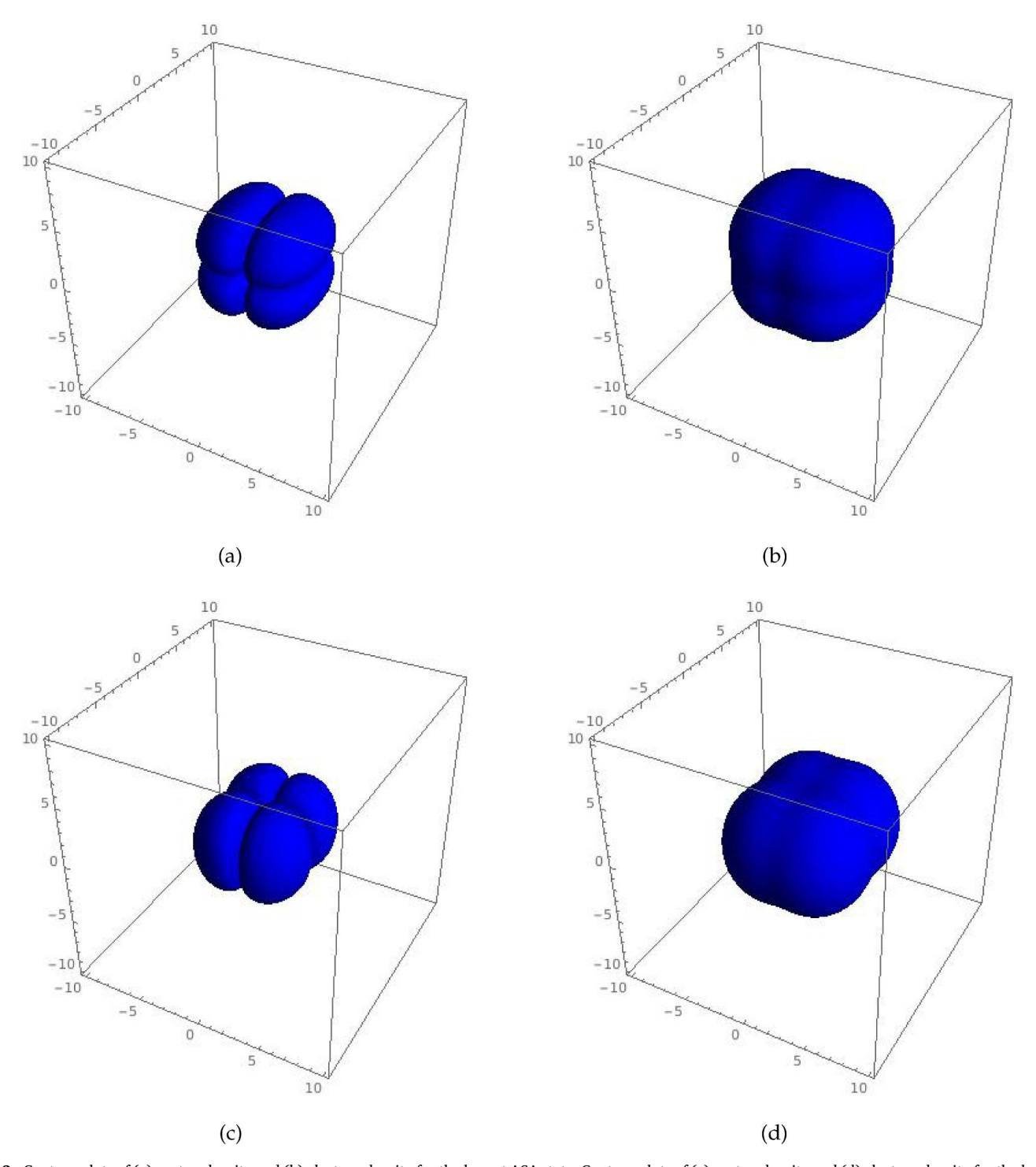


Fig. 3. Contour plots of (a) proton density and (b) electron density for the lowest ASA state; Contour plots of (c) proton density and (d) electron density for the lowest ASA state. The contour value used in plots (a)-(c) is 0.0003.

density to any appreciable extent. Therefore, it can be safely concluded that a grid size of 0.5 a.u. along all the different axes is a good one. Hence, we used this particular grid size in all our calculations for both the ground and excited states that will be presented next.

One of the important features in the density plots is the appearance of radial nodes. For the SSS case, since the wave function is symmetric with respect to reflection along all three planes, we do not expect to find a nodal plane, so both the electronic and nuclear densities look like an ellipsoid that is slightly elongated along the longest axial direction (the y-axis in our case). For the cases with one nodal plane, namely, the ASS, SAS, and SSA cases, we would expect to find one nodal plane along the

plane where the wave function is antisymmetric with respect to reflection. In the ASS case, this nodal plane is the x-plane. Similarly, the SAS case exhibits a nodal plane along the y-plane and for the SSA case, the nodal plane is the z-plane. Along a similar vein, one would expect two nodal planes in the AAS, ASA, and SAA cases, since all these angular symmetry cases have two different antisymmetric planes with respect to reflection. The AAS case has the x and y-planes as its nodal planes, the ASA case has nodal planes in the x and z planes and for the SAA case, the nodal planes appear in the y and z planes simultaneously. Finally, the AAA case calculations show three mutually perpendicular nodal planes, namely all the axial planes.

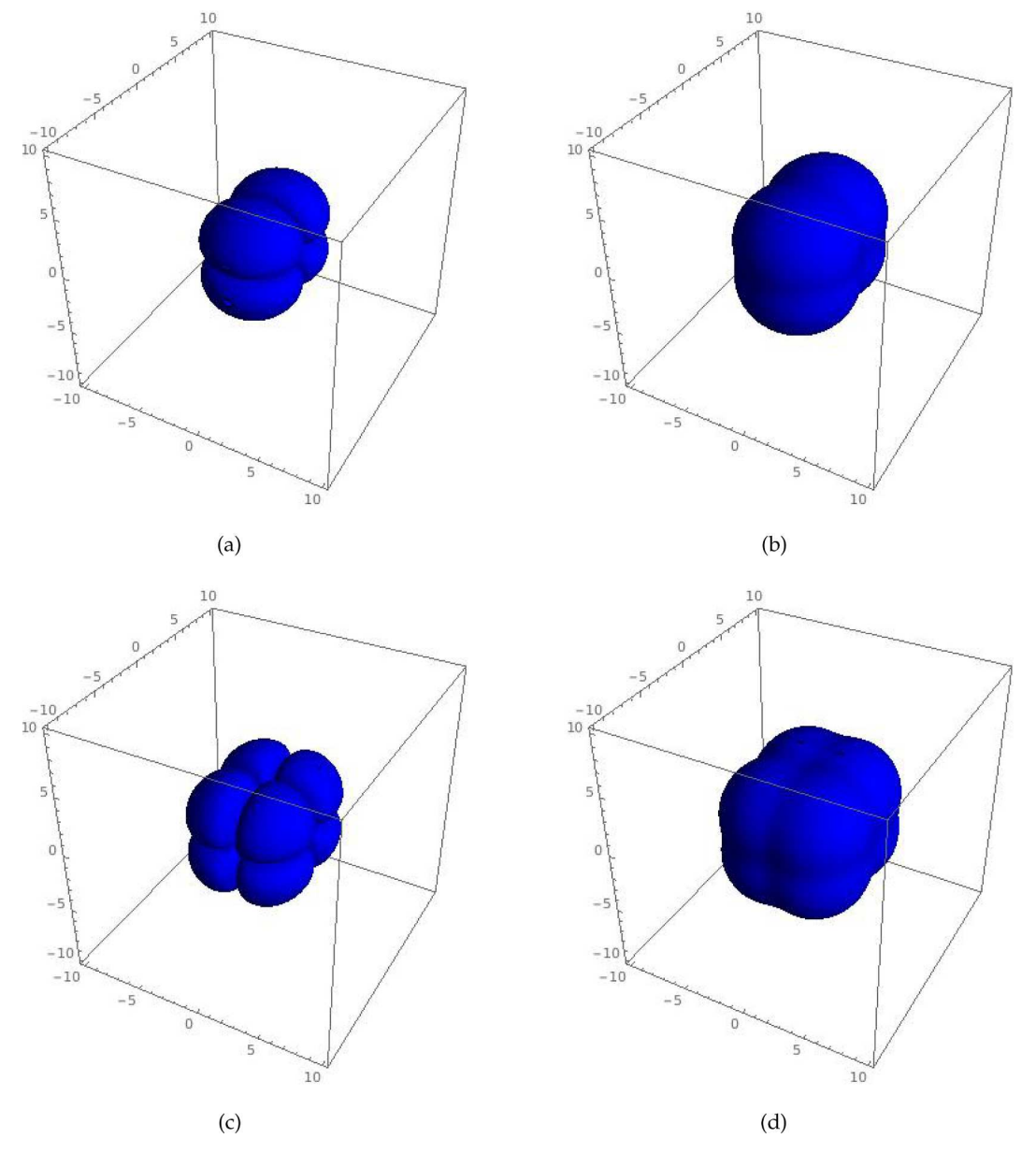


Fig. 4. Contour plots of (a) proton density and (b) electron density for the lowest SAA state; Contour plots of (c) proton density and (d) electron density for the lowest SAA state. The contour value used in plots (a)-(c) is 0.0003.

Another feature of importance in our density diagrams is the difference in volume (diffusion) and sharpness of the boundaries of the nodal planes for the nuclear and electronic densities. This is in accordance with what can be expected. Since the electron is much lighter than the proton it gives rise to a more diffused particle density than the proton.

The next part of this work focuses on discussing the calculations done to describe "radial" spreading of the hydrogen-atom wave functions throughout the cuboid box (we will call the corresponding states the translational states). It should be realized that, if a sufficiently complete basis set is used in the calculation, the spreading should happen as a result of the variational minimization of the hydrogen-atom total energy. This would happen because the spreading lowers the kinetic energy of the center-of-mass motion of the hydrogen atom as a whole. However, if a small basis set is used (as is done in the present calculations), the main energy gain in the minimization comes from improving the internal energy and the corresponding wave function of the hydrogen atom rather than from spreading the non-BO wave function of the atom throughout the box.

To study the translational states of the hydrogen atom in the box, we start with three optimized generator Gaussian functions obtained from the calculations of the lowest energy state for each of the eight symmetries, i.e. SSS, ASS, SAS, SSA, ..., etc. Then, for each symmetry, we make 23 copies of each of these generator Gaussians. In these copies, the  $L_k$  values of the wave functions remain the same, but we shift the generator Gaussians  $s_k$  vector by adding a spreading factor a. The diffusion of the generator Gaussians along the three axes is done in such a way that we have the most function copies along the longest axis (y-axis) and the least copies along the shortest axis (x-axis). In our calculations, we chose to have only one copy along the x-axis (a), three copies along the y-axis (a, 2a, and 3a) and two copies along the z-axis (a and 2a). If the coordinates of the  $s_k$  vector of a generator Gaussian function are (x1,y1,z1,x2,y2,z2), the above-mentioned procedure will yield the following 23 copies (or 24 copies when the generator copy is included):

$$(x1+a, y1, z1, x2+a, y2, z2)$$

$$(x1, y1 + a, z1, x2, y2 + a, z2)$$

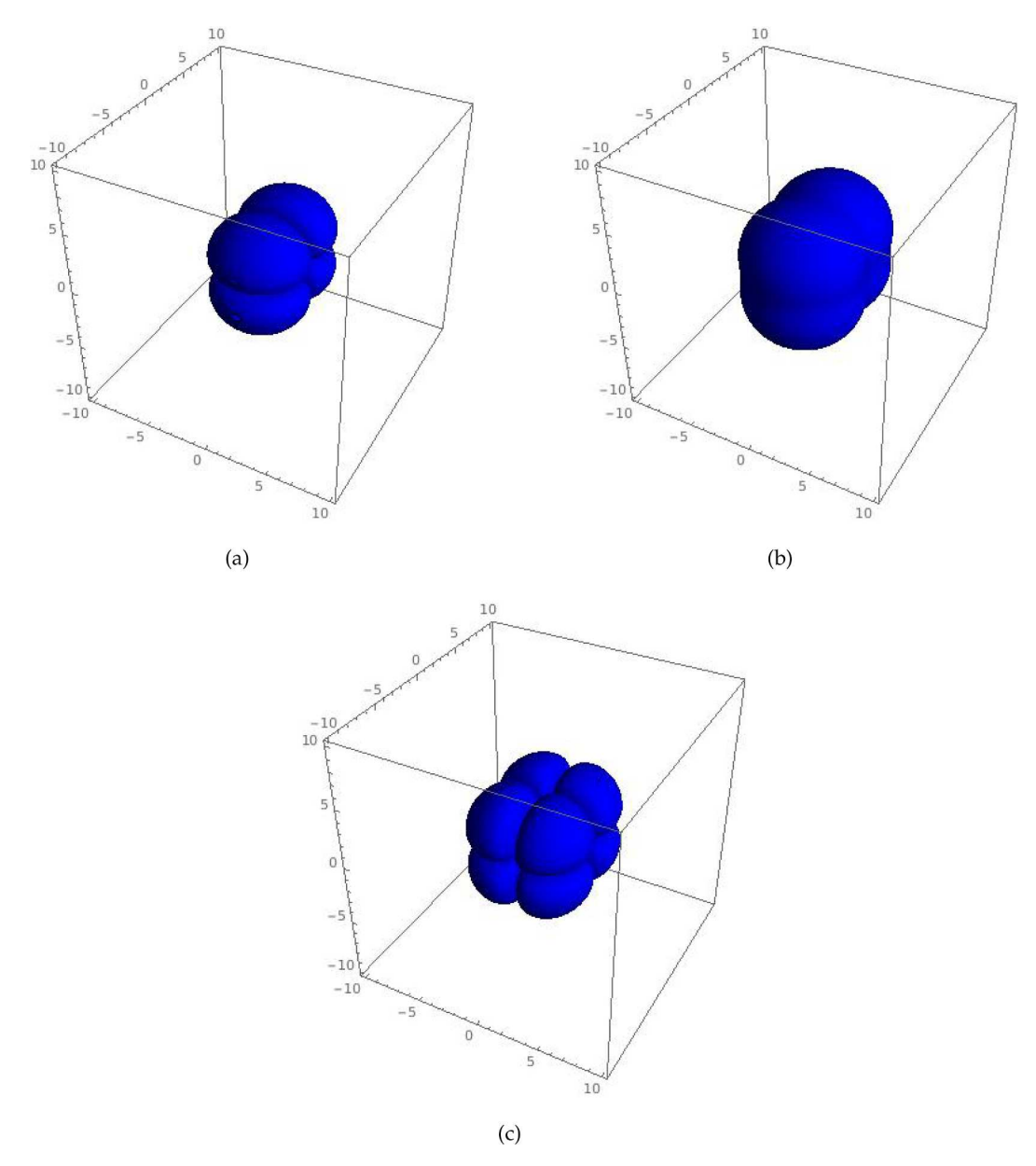


Fig. 5. Contour plots of the proton density of the translational states for the SSS symmetry. (a) shows the lowest energy state, (b) shows state 5, and (c) shows state 24.

Table 2
The integrated proton densities corresponding to the eight different angular symmetries of the wave function of the confined hydrogen atom.

The state of the s		
Angular Symmetry State	Integrated Density (Proton)	
SSS	0.9999999999981	
SAS	0.99999999999971	
SSA	0.99999999999978	
ASS	0.99999999999963	
ASA	0.9999999998882	
AAS	0.99999999999967	
SAA	0.9999999999978	
AAA	0.9999999999884	

$$(x1, y1 + 2a, z1, x2, y2 + 2a, z2)$$

$$(x1, y1 + 3a, z1, x2, y2 + 3a, z2)$$

$$(x1, y1, z1 + a, x2, y2, z2 + a)$$

**Table 3**The integrated electron densities corresponding to the eight different angular symmetries of the wave function of the confined hydrogen atom.

Integrated Density (Electron)
0.99999994
0.99999926
0.99999983
0.99999986
0.99999239
0.99999928
0.99999818
0.99999555

$$(x1, y1, z1 + 2a, x2, y2, z2 + 2a)$$

$$(x1+a, y1+a, z1, x2+a, y2+a, z1)$$

$$(x1+a, y1+2a, z1, x2+a, y2+2a, z1)$$

**Table 4** Optimum values of the spreading factor a for the eight angular symmetry cases for hydrogen atom.

Angular Symmetry State	Optimum a value (in a.u.)
SSS	2.8
SAS	2.6
SSA	2.7
ASS	2.7
ASA	2.5
AAS	2.4
SAA	2.5
AAA	2.5

$$(x1+a, y1+3a, z1, x2+a, y2+3a, z1)$$

$$(x1+a, y1, z1+a, x2+a, y2, z1+a)$$

$$(x1+a, y1, z1+2a, x2+a, y2, z1+2a)$$

$$(x1, y1 + a, z1 + a, x2, y2 + a, z1 + a)$$

$$(x1, y1 + 2a, z1 + a, x2, y2 + 2a, z1 + a)$$

$$(x1, y1 + 3a, z1 + a, x2, y2 + 3a, z1 + a)$$

$$(x1, y1 + a, z1 + 2a, x2, y2 + a, z1 + 2a)$$

$$(x1, y1 + 2a, z1 + 2a, x2, y2 + 2a, z1 + 2a)$$

$$(x1, y1 + 3a, z1 + 2a, x2, y2 + 3a, z1 + 2a)$$

$$(x1+a, y1+a, z1+a, x2+a, y2+a, z1+a)$$

$$(x1+a, y1+2a, z1+a, x2+a, y2+2a, z1+a)$$

$$(x1+a, y1+3a, z1+a, x2+a, y2+3a, z1+a)$$

$$(x1+a, y1+a, z1+2a, x2+a, y2+a, z1+2a)$$

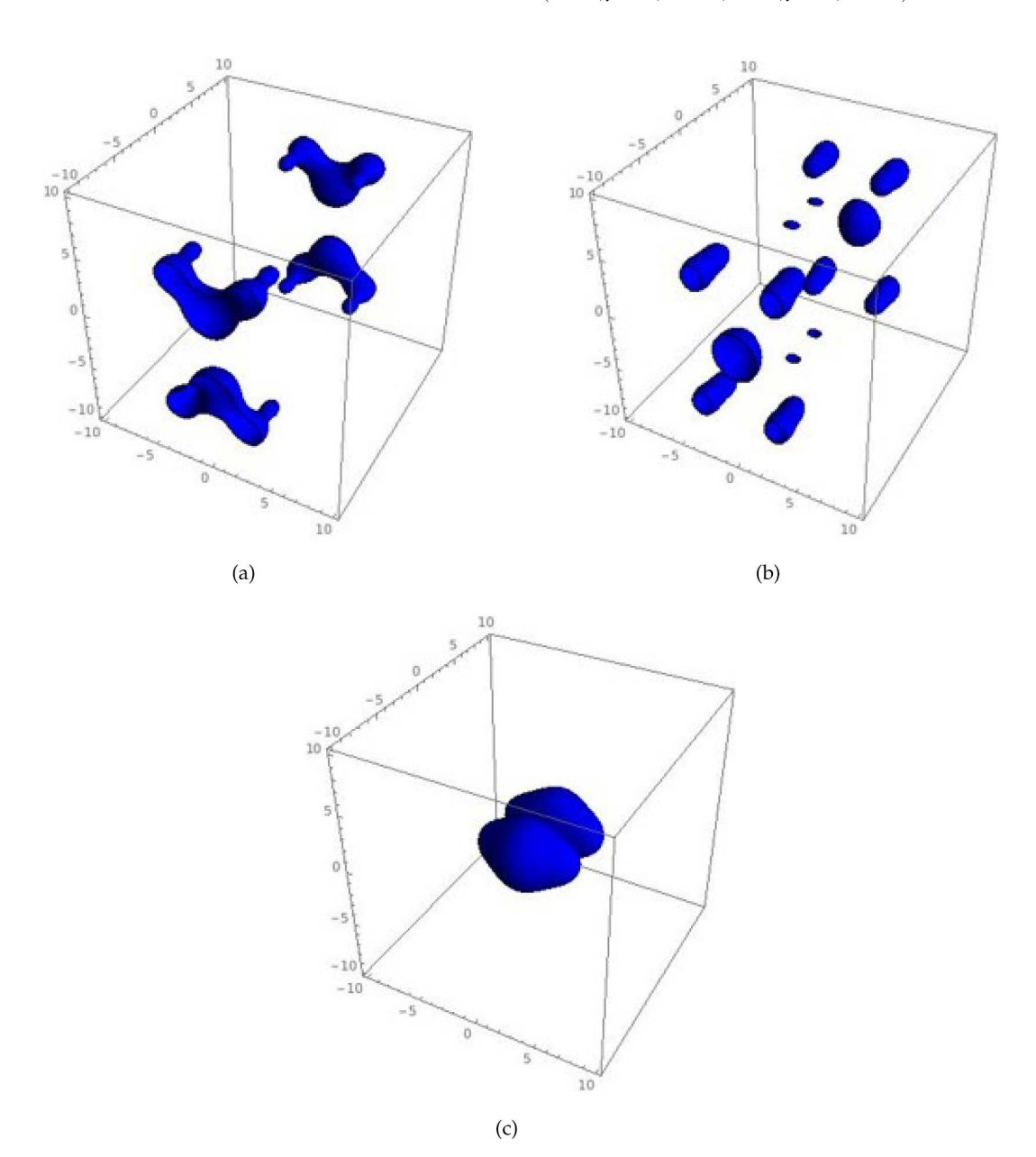


Fig. 6. Contour plots of the proton density of the translational states for the SAS symmetry. (a) shows the lowest energy state, (b) shows state 5, and (c) shows state 24.

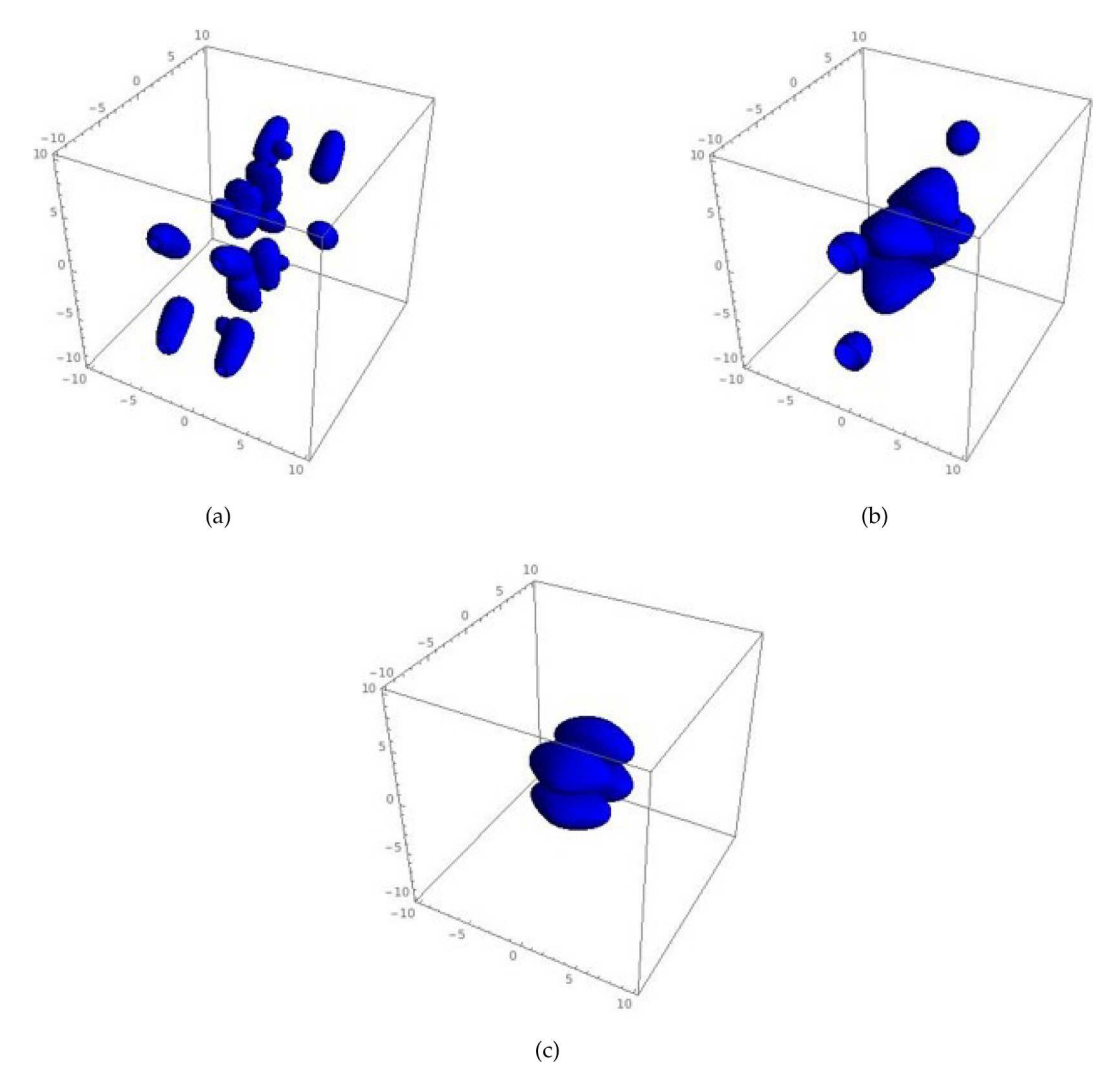


Fig. 7. Contour plots of the proton density of the translational states for the SAA symmetry. (a) shows the lowest energy state, (b) shows state 5, and (c) shows state 24.

$$(x1+a, y1+2a, z1+2a, x2+a, y2+2a, z1+2a)$$

$$(x1+a, y1+3a, z1+2a, x2+a, y2+3a, z1+2a)$$

As one notices, in the first set of 6 functions, the spreading factor is added to one axial direction at a time. In the next set of 11 functions, the expansion is simultaneously carried out in two axial directions, and in the last set of 6 functions, we expand along all three axial directions at the same time. When we apply this method to the three starting generator functions, we get  $3\times 24=72$  Gaussian copies. It should also be noted here that the 72 Gaussians are symmetry adapted for each of the eight angular symmetries to give us a total of  $72\times 8=576$  Gaussians that fill up all the space inside the "box".

This method of spreading the three generator Gaussians throughout the box can simulate the translational motion (i.e. translational bound states) of the H-atom system within the box, as if the H-atom is "moving" from point-to-point within the confines of the box. Thus, we can approximately describe the translational ground and excited states of the system by using this method.

Our next task is to find an optimum value of this spreading factor a for all the eight angular symmetry cases. For this purpose, we choose values of a between 0.5 and 3.0 a.u. in increments of 0.1 a.u. and calculate the sum of the energies of the 24 lowest states of the system. The value of a that gives us the least energy sum is chosen as the optimum value for that particular angular symmetry case. We choose to

optimize the energy sum of 24 states since there are 24 copies of a single generator Gaussian and the spacing between the energy levels of these 24 lowest energy states is too low for us to be able to access them individually in the minimization process.

Values of a less than 0.5 a.u were too small to spread the functions effectively and by creating linear dependencies caused our optimization routine to fail. Values of a higher than 3 a.u. on the other hand, moved the centers of the expanded Gaussians outside the "box" giving unrealistic energy values. In the Table 4, we have tabulated the optimum values of the spreading factor a for all eight angular symmetry cases.

Once the optimum value of a is determined, we calculate the densities using the wave functions of the translational ground and excited states of the system. These densities show how the electron and proton clouds are distributed in the box in each of the 24 lowest energy states for the eight angular symmetries. The Fig. 5–8 show the proton densities of some of the energy levels of the translational excited states for a few of the angular symmetry cases. The proton densities are much sharper and less diffused than the electron densities as shown previously and this is why we chose to plot the proton densities in the excited state calculations. Although we have prepared these proton density diagrams for all the eight states, we present only a few representative cases here for illustrative purposes. Fig. 5(a) - (c) represents the translational fully symmetric SSS states 1, 5, and 24. The SAS case is randomly chosen as a "test-case" of a state with one antisymmetry plane. Fig. 6(a) - (c) show the energy levels 1, 5, and 24 for this particular SAS case. To illustrate

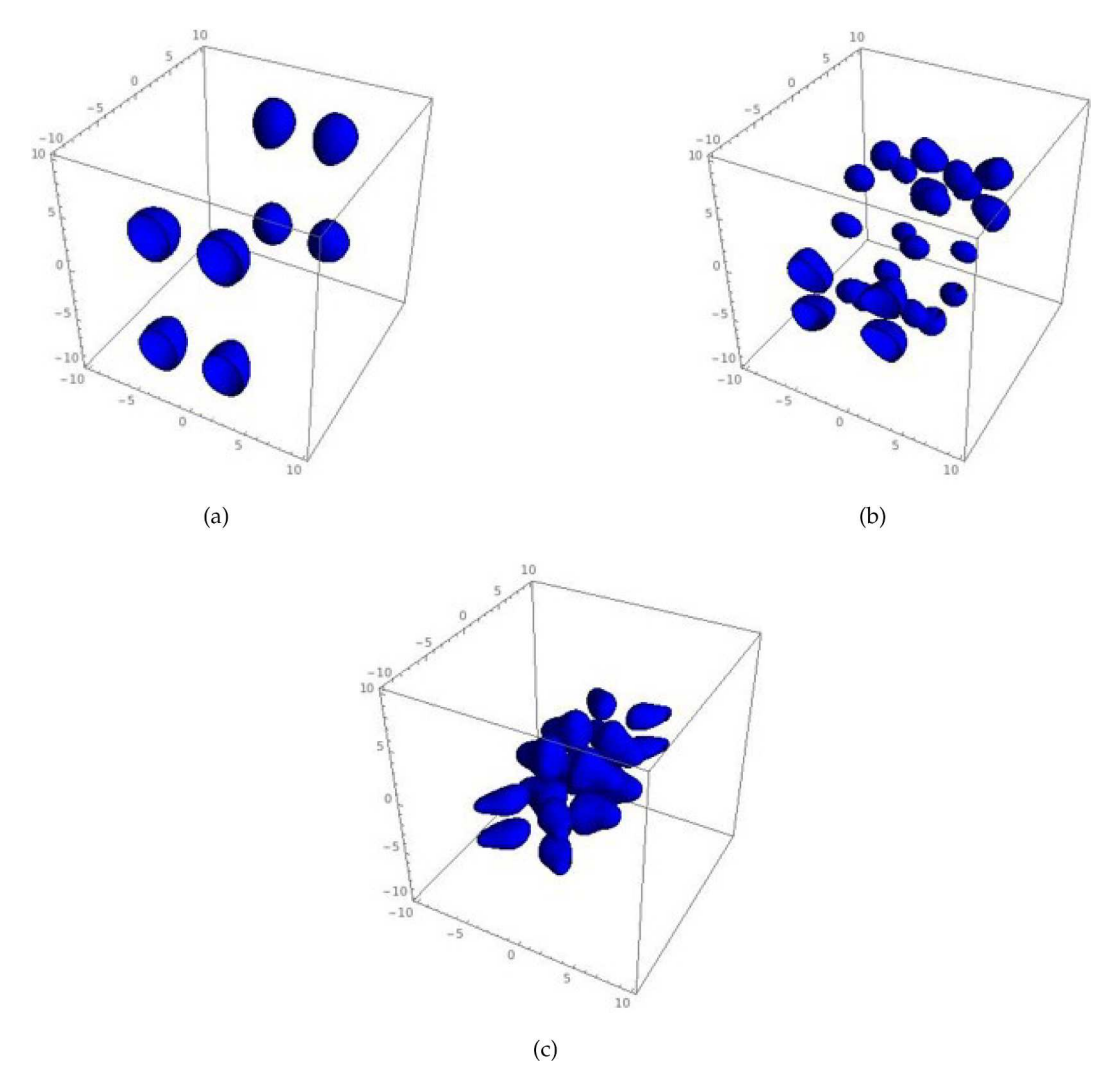


Fig. 8. Contour plots of the proton density of the translational states for the AAA symmetry. (a) shows the lowest energy state, (b) shows state 5, and (c) shows state 24.

what happens when we have 2 antisymmetry planes in the angular symmetry, we choose the "test-case" of the SAA state and in Fig. 7(a) - (c), the density plots for the energy levels 1, 5 and 24 of the said SAA case are presented. Finally, we show the energy levels for the translationally excited AAA case, which has three antisymmetry planes. In Fig. 8(a) - (c), the density plots corresponding to energy levels 1, 5 and 24 with the AAA symmetry are shown.

There are a couple of important takeaways from Fig. 5(a) - 8(c). First is the fact that the wave functions in energy levels 1, 5 and 24 are visibly very different. The difference results from mutual orthogonality of the wave functions of the states within the same angular symmetry. The second important feature that is apparent in the plots is that, as the energy of the level increases, the wave function becomes more localized within the box. Therefore, state 1 which has the lowest energy is the most delocalized and exhibits the most tunneling whereby the wave function seeps outside the box. State 24 on the other hand, which has the highest energy, also has the most localized wave function. As the result of the strong localization of this state, its integrated proton and electron densities are closer to one than for the other states. The stronger localization of the higher excited states than of the lower laying states results from a larger center-of-mass kinetic energy that is a part of the total energy of each state.

# 4. Conclusions

A computational model to study bound states of a hydrogen atom placed in a cuboidal potential energy trap is proposed, implemented, and tested. The wave functions for the ground and excited states of the system are expanded using all-particle explicitly correlated Gaussian functions with shifted centers. The variational method is used to optimize the non-linear parameters of the Gaussians. The explicitly correlated Gaussian functions allow us to more accurately represent the electron-electron, electron-nucleus, and nucleus-nucleus correlation effects much better than obtained with an approach that employs electronic and nuclear orbitals. Naturally, for the hydrogen atom, only the first of the three correlations is present.

Eight possible angular symmetries of the wave function in the trapping potential of a cuboidal box formed by alternating point charges are examined. For each symmetry, both ground and excited states are calculated. The excited states, which are called translational states, correspond to the different ways the hydrogen atom delocalizes within the PE trap. One-particle density plots are used to visualize the results. They show the physical nature of the states.

The non-Born-Oppenheimer approach that treats both the nuclei and electrons on a equal footing presented in this "proof-of-concept" study for the test case of a trapped hydrogen atom will be applied to study various other systems under the same trapping potential. Work is currently underway to extend the approach to a trapped hydrogen

molecule and to a system of multiple hydrogen molecules trapped within the cuboidal box. At a later stage, we would also like to expand our studies to simulate a more realistic PE trap comprises real molecules rather than point charges, as presented in this work. Various applications of the present method will continue to be an important focus of our upcoming future research.

## **Data Availability**

The data that support the findings of this study are available from the corresponding author upon request.

#### **Declaration of Competing Interest**

The authors declare that they have no known competing financial interests or personal relationships that could have appeared to influence the work reported in this paper.

#### Acknowledgements

This work has been supported by a grant from the National Science Foundation; Grant No. 1856702. L. A. acknowledges the support of the Centre for Advanced Study (CAS) in Oslo, Norway, which funds and hosts our research project titled: Attosecond Quantum Dynamics Beyond the Born-Oppenheimer Approximation, during the 2021–22 academic year.

#### References

- [1] E. Ley-Koo, S.A. Cruz, The hydrogen atom and the  ${\rm H_2^+}$  and  ${\rm HeH^{++}}$  molecular ions inside prolate spheroidal boxes, J. Chem. Phys. 74 (8) (1981) 4603–4610.
- [2] J. Gorecki, W. Byers Brown, On the ground state of the hydrogen-molecule ion H<sup>1</sup><sub>2</sub> enclosed in hard and soft spherical boxes, J. Chem. Phys. 89 (4) (1988) 2138–2148.
- [3] S. Mateos-Cortés, E. Ley-Koo, S.A. Cruz, Hydrogen molecular ion inside penetrable prolate spheroidal boxes: Electronic and vibrational properties, Int. J. Quantum Chem. 86 (4) (2002) 376–389.
- [4] E. Ley-Koo, The hydrogen atom confined in semi-infinite spaces limited by conoidal boundaries, in: Advances in Quantum Chemistry, vol. 57, Academic Press, 2009, pp. 79–122.
- [5] R. Colín-Rodríguez, C. Díaz-García, S.A. Cruz, The hydrogen molecule and the H<sup>+</sup><sub>2</sub> molecular ion inside padded prolate spheroidal cavities with arbitrary nuclear positions 44(24) (2011) 241001.
- [6] C.A. Ten Seldam, S.R. De Groot, On the ground state of a model for compressed helium, Physica 18 (11) (1952) 891–904.
- [7] C.A. Ten Seldam, S.R. De Groot, On the polarizability of a model of the compressed helium atom, Physica 18 (11) (1952) 905–909.
- [8] H.E. Montgomery, N. Aquino, A. Flores-Riveros, The ground state energy of a helium atom under strong confinement, Phys. Lett. A 374 (19) (2010) 2044–2047.
- [9] S. Waugh, A. Chowdhury, A. Banerjee, On the variation of polarizability and hyperpolarizability of a confined atom with the strength of confinement: A case study of a helium atom, J. Phys. B: At. Mol. Phys. 43 (22) (2010) 225002.
- [10] W.S. Nascimento, M.M. de Almeida, F.V. Prudente, Coulomb correlation and information entropies in confined helium-like atoms, Eur. Phys. J. D 75 (6) (2021).
- [11] A. Robles-Navarro, M. Rodriguez-Bautista, P. Fuentealba, C. Crdenas, The change in the nature of bonding in the li<sub>2</sub> dimer under confinement, Int. J. Quantum Chem. 121 (12) (2021).
- [12] S. Lumb, S. Lumb, V. Prasad, D. Sugny, Effect of electric field on thermodynamic properties of confined molecules, Chem. Phys. 510 (2018) 37–46.
- [13] S. Lumb, S. Lumb, V. Prasad, Photoexcitation and ionization of a hydrogen atom confined by a combined effect of a spherical box and debye plasma, Phys. Lett. A 379 (18) (2015) 1263–1269.
- [14] P.C. Bhowmik, F. Yadav, R.N. Singh, A. Goyal, M. Mohan, Effect of plasma environment on spectral and structural properties of H-like C, N and O ions, J. Electron. Spectrosc. Relat. Phenom. 251 (2021) 147107.
- [15] F.N. El-Gammal, Confined atoms in plasma environment: variational monte carlo calculations, Mol. Phys. 119 (8) (2021).
- [16] S.J.C. Salazar, H.G. Laguna, V. Prasad, R.P. Sagar, Shannon-information entropy sum in the confined hydrogenic atom, Int. J. Quantum Chem. 120 (11) (2020).
- [17] R. Vawter, Effects of finite boundaries on a one-dimensional harmonic oscillator, Phys. Rev. 174 (1968) 749–757.
- [18] S. LumbTalwar, S. Lumb, V. Prasad, Charge currents and induced magnetic fields in a bounded two-dimensional hydrogen atom, Eur. Phys. J. D 75 (2) (2021).

- [19] V. Prasad, S. Lumb Talwar, S. Lumb, G. Lefkidis, and W. Hbner. Persistent currents and induced magnetization in presence of external magnetic field and transition probabilities in presence of combined laser pulse and external magnetic field for a confined hydrogen atom, Phys. Lett. Sect. A: General Atom. Solid State Phys. 383 (26) (2019).
- [20] E.A. Koval, O.A. Koval, Anisotropic features of two-dimensional hydrogen atom in magnetic field, J. Exp. Theor. Phys. 125 (1) (2017) 35–42.
- [21] B. Suryan, Bounded linear harmonic oscillator and phase transitions of second order, Phys. Rev. 71 (1947) 741–742.
- [22] M.F. Morcillo, J.M. Alcaraz-Pelegrina, A. Sarsa, Ionisation and excitation probabilities of a hydrogen atom suddenly released from penetrable confinement, Mol. Phys. 117 (13) (2019) 1621–1628.
- [23] T. Sako, G.H.F. Diercksen, Confined quantum systems: A comparison of the spectral properties of the two-electron quantum dot, the negative hydrogen ion and the helium atom, J. Phys. B: At. Mol. Opt. Phys. 36 (9) (2003) 1681–1702.
- [24] P. Dean, The constrained quantum mechanical harmonic oscillator, Math. Proc. Cambridge Philos. Soc. 62 (2) (1966) 277–286.
- [25] E. Caurier, G. Martínez-Pinedo, F. Nowacki, A. Poves, A.P. Zuker, The shell model as a unified view of nuclear structure, Rev. Mod. Phys. 77 (2005) 427–488.
- [26] A. Michels, J. De Boer, A. Bijl, Remarks concerning molecural interaction and their influence on the polarisability, Physica 4 (10) (1937) 981–994.
- [27] J.A. Weil, Hydrogen atom in a spherical box. ii. effect on hyperfine energy of excited state admixture, J. Chem. Phys. 71 (7) (1979) 2803–2805.
- [28] S. Lumb, S. Lumb, K.D. Sen, V. Prasad, Effect of dipole moments on orientation and alignment of a bounded molecule, J. Mol. Struct. 1137 (2017) 300–309.
- [29] D. Suryanarayana, J.A. Weil, On the hyperfine splitting of the hydrogen atom in a spherical box, J. Chem. Phys. 64 (2) (1976) 510–513.
- [30] E.V. Ludena, SCF calculations for hydrogen in a spherical box, J. Chem. Phys. 66 (2) (1977) 468–470.
- [31] E. Ley-Koo, S. Rubinstein, The hydrogen atom within spherical boxes with penetrable walls, J. Chem. Phys. 71 (1) (1979) 351–357.
- [32] E. Ley-Koo, S. Rubinstein, The hydrogen atom inside boxes with paraboloidal surfaces, J. Chem. Phys. 73 (2) (1980) 887–893.
- [33] T. Novoa, J. Contreras-Garca, P. Fuentealba, C. Crdenas, The Pauli principle and the confinement of electron pairs in a double well: Aspects of electronic bonding under pressure, J. Chem. Phys. 150 (20) (2019) 204304.
- [34] U. Sarkar, S. Giri, P.K. Chattaraj, Dirichlet boundary conditions and effect of confinement on chemical reactivity, J. Phys. Chem. A 113 (40) (2009) 10759–10766.
- [35] V.D. Burkert, L. Elouadrhiri, F.X. Girod, The pressure distribution inside the proton. Nature 557 (2018) 396–399.
- [36] C. Laughlin, B.L. Burrows, M. Cohen, A hydrogen-like atom confined within an impenetrable spherical box 35(3) (2002) 701–715.
- [37] H.O. Batael, E.D. Filho, Ground-state energy for confined H<sub>2</sub>: a variational approach, Theoret. Chem. Acc. 137 (65) (2018) 438.
- [38] L.F. Pateka, T. Helgaker, T. Saue, D. Sundholm, H.J. Werner, M. Hasanbulli, J. Major, P. Schwerdtfeger, Atoms and molecules in soft confinement potentials, Mol. Phys. 118 (19–20) (2020) e1730989.
- [39] P.M. Kozlowski, L. Adamowicz, Equivalent quantum approach to nuclei and electrons in molecules, Chem. Rev. 93 (6) (1993) 2007–2022.
- [40] G.W. Crabtree, M.S. Dresselhaus, M.V. Buchanan, The hydrogen economy, Phys. Today 57 (12) (2004) 39–44.
- [41] A. Schneemann, J.L. White, S. Kang, S. Jeong, L.F. Wan, E.S. Cho, T.W. Heo, D. Prendergast, J.J. Urban, B.C. Wood, M.D. Allendorf, V. Stavila, Nanostructured metal hydrides for hydrogen storage, Chem. Rev. 118 (22) (2018) 10775–10839.
- [42] A. Zttel, Materials for hydrogen storage, Mater. Today 6 (9) (2003) 24–33.
- [43] S. Niaz, T. Manzoor, A.H. Pandith, Hydrogen storage: Materials, methods and perspectives, Renew. Sustain. Energy Rev. 50 (2015) 457–469.
- [44] A. Gupta, G.V. Baron, P. Perreault, S. Lenaerts, R.G. Ciocarlan, P. Cool, P.G. M. Mileo, S. Rogge, V. Van Speybroeck, G. Watson, P. Van Der Voort, M. Houlleberghs, E. Breynaert, J. Martens, J.F.M. Denayer, Hydrogen clathrates: Next generation hydrogen storage materials, Energy Storage Mater. 41 (2021) 69–107.
- [45] M. Cafiero, L. Adamowicz, Non-bornoppenheimer molecular structure and one-particle densities for  $\rm H_2D^+$ , J. Chem. Phys. 122 (18) (2005) 184305.
- [46] Cecil Laughlin, Shih-I Chu, A highly accurate study of a helium atom under pressure, J. Phys. A: Math. Theor. 42 (26) (2009) 265004.
- [47] S. Bhattacharyya, J.K. Saha, P.K. Mukherjee, T.K. Mukherjee, Precise estimation of the energy levels of two-electron atoms under spherical confinement, Phys. Scr. 87 (6) (2013) 065305.
- [48] S. Bhattacharyya, J.K. Saha, T.K. Mukherjee, Nonrelativistic structure calculations of two-electron ions in a strongly coupled plasma environment, Phys. Rev. A 91 (2015) 042515.
- [49] Li Guang Jiao, Li Rong Zan, Yong Zhi Zhang, Yew Kam Ho, Benchmark values of Shannon entropy for spherically confined hydrogen atom, Int. J. Quantum Chem. 117 (13) (2017) e25375.
- [50] Keith Jones, Explicitly Correlated Gaussian Functions and Rovibrational Spectra of Diatomic Molecules (PhD thesis), The University of Arizona, 2018.